Ren *et al. Biochar* (2024) 6:20
https://doi.org/10.1007/s42773-023-00297-9

Biochar

ORIGINAL RESEARCH Open Access

Variable frequency microwave induced CO_2 Boudouard reaction over biochar

Jurong Ren[1,2], Jianchun Jiang[1,2*], Jia Wang[1,2*], Xiangzhou Yuan[3] and Ao Wang[1]

Abstract

The Boudouard reaction presents promising application prospects as a straightforward and efficient method for CO_2 conversion. However, its advancement is hindered primarily by elevated activation energy and a diminished conversion rate. This study employed a microwave reactor with a variable frequency as the initial approach to catalyze the CO_2 Boudouard reaction over biochar, with the primary objective of producing renewable CO. The study systematically investigated the influence of various variables, including the heating source, microwave frequency, microwave power, gas hourly space velocity (GHSV), and carrier gas, on the conversion of CO_2 and the selectivity towards CO. The experimental findings indicate that under static conditions, with a fixed microwave frequency set at 2450 MHz and 100 W microwave power, the Boudouard reaction did not initiate. Conversely, a CO_2 conversion rate of 8.8% was achieved when utilizing a microwave frequency of 4225 MHz. Under this unique frequency, further elevating the microwave power to 275 W leads to the complete conversion of CO_2. Furthermore, a comparative analysis between microwave and electrical heating revealed that the CO production rate was 37.7 μmol kJ^{-1} for microwave heating, in stark contrast to the considerably lower rate of 0.2 μmol kJ^{-1} observed for electric heating. Following the reaction, the biochar retained its robust 3D skeleton structure and abundant pore configuration. Notably, the dielectric constant increased by a factor of 1.8 compared to its initial state, rendering it a promising microwave-absorbing material.

Highlights

- A microwave reactor with a variable frequency was utilized to perform the CO_2 Boudouard reaction to produce CO.
- A CO_2 conversion of 100% could be maintained for more than 100 min at the microwave frequency of 4225 MHz.
- The CO_2 conversion of microwave heating was 96.4% higher than that of conventional electric heating.
- Renewable biochar served a dual purpose as both an adsorbent and raw material in this study, with the reacted biochar demonstrating efficacy as a proficient absorbing material.

Keywords Variable microwave frequency, Boudouard reaction, CO_2 conversion, Biochar

Handling editor: Xiangzhou Yuan.

*Correspondence:
Jianchun Jiang
jiangjc@caf.ac.cn
Jia Wang
wangjia@njfu.edu.cn
Full list of author information is available at the end of the article

Graphical Abstract

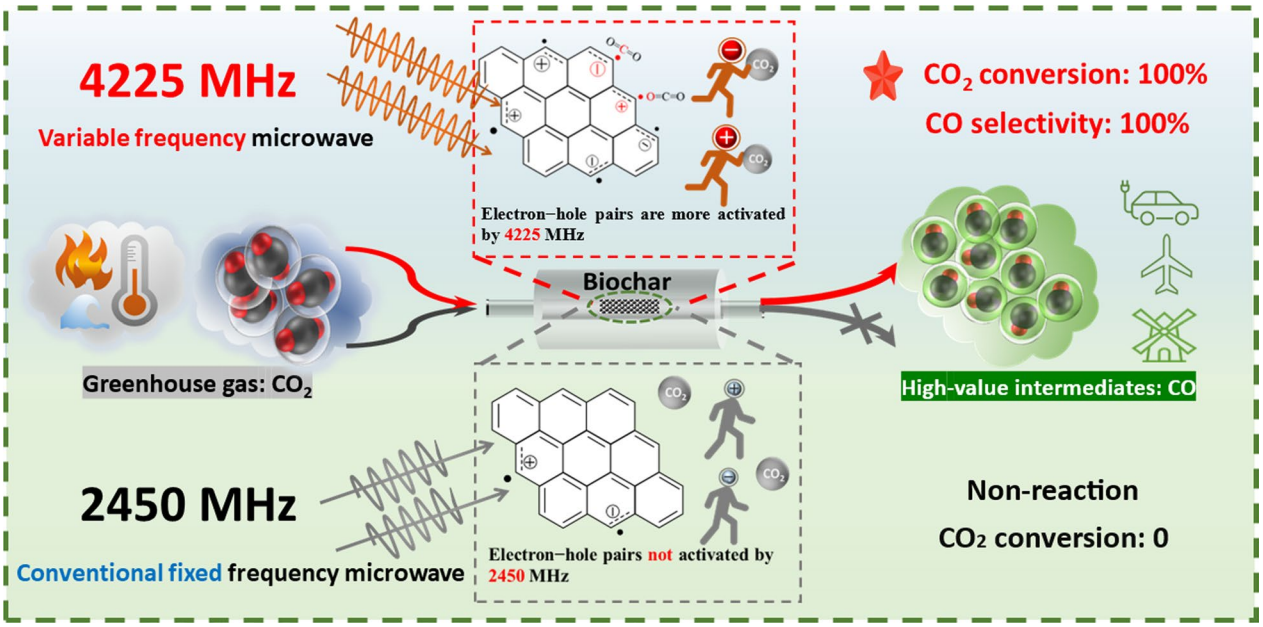

1 Introduction

The escalating consumption of fossil fuels and the consequential release of substantial greenhouse gas emissions have engendered severe energy crises and exacerbated global warming issues. With the ongoing development of the economy and modern industries, there is a continual expansion of energy demand, concomitant with a notable increase in greenhouse gas emissions (Yuan et al. 2023). Carbon dioxide (CO_2), a pivotal constituent of greenhouse gases, exerts a pronounced impact on the ecological environment (Yuan et al. 2021), precipitating an elevation in the global average temperature and sea level. Furthermore, the emissions of greenhouse gases disrupt the growth environment for animals and plants, leading to ecological imbalances and presenting a formidable challenge to species diversity. Consequently, the development of technology for the capture, storage, transformation, and utilization of CO_2 has become a shared concern within the contemporary scientific community (Vakalis et al. 2018).

In contrast, carbon monoxide (CO) serves as an indispensable foundational material in organic synthesis, contributing to the production of diverse organic chemicals, including methanol, formamide, dimethylformamide, methyl formatted, and acetic acid (Medrano-García et al. 2019; Luo et al. 2023). The reduction of carbon dioxide (CO_2) to CO represents a transformative approach to converting greenhouse gases into intermediates for the synthesis of high-value-added chemicals (Bai et al. 2017). Strategies for CO_2 conversion encompass various methodologies, primarily electrochemical, photochemical, and thermochemical methods (Ishida et al. 2020). Notably, electrochemical reduction of CO_2 is acknowledged as a clean and sustainable technology (Jin et al. 2021). Xuan et al. (2022) innovatively designed a tertiary amine-functionalized Co(II) porphyrin (2NPorCo) catalyst for electrochemical CO_2 reduction, achieving a remarkable CO Faraday efficiency of 96.7%, coupled with a turnover rate of 5433 h^{-1}. However, the process necessitates a complex catalytic system, and its energy efficiency is constrained by the substantial overpotential required for CO_2 activation. Additionally, the CO_2 reduction process is intricate, involving the transfer of multiple protons and electrons, resulting in diverse product outcomes. The similarity in thermodynamic redox potentials among these outcomes contributes to limited selectivity (Zhao and Quan 2021).

Photocatalytic CO_2 reduction is an emerging technology that utilizes solar energy to convert CO_2 into high-value products, possessing the characteristics of being green and renewable (Guo et al. 2023). It serves the dual purpose of solar energy fixation and CO_2 emission reduction (Zhai et al. 2023). Fu et al. (2023) conducted a study on a prepared heterostructure catalyst based on the Z-type bismuth perovskite, exhibiting remarkable

attributes, including high charge separation and potent redox capability. This catalyst is aimed at photocatalytic CO_2 reduction, achieving an optimal CO yield of up to 98.9 μmol g^{-1} h^{-1}. Nevertheless, the efficiency of photocatalytic CO_2 reduction remains restricted due to the limited range of light absorption. Consequently, the current efficiency of the photocatalytic reaction is far from meeting the demands of industrial-scale production (Wang et al. 2022). Additionally, the practical application of this process could also be hindered by challenges related to the availability and the cost of catalyst materials (Ishida et al. 2020).

On the other hand, the thermal catalytic reduction of CO_2 has the unique advantage of high CO_2 conversion and multiple target products can be harvested (Chan et al. 2021). The possibility of CO_2 reduction through the reverse water gas shift reaction has been established. Liu et al. (2021) formulated a catalyst denoted as 1% Ni/SBA-15(P), recognizing for its high CO_2 conversion efficiency and robust stability in the reaction. Under a temperature of 700 °C, the CO_2 conversion reached 33.7%. Jensen et al. (2021) prepared 10wt%Ni2wt%Pd0.1wt%Ir/$CeZrO_2$ catalysts and used them for the reverse water gas conversion reaction at high temperatures. The deliberate synergy between the metals and the catalyst support results in a significant improvement in the efficiency of CO_2 hydro-reduction, ultimately reaching a remarkable 52.4% conversion rate. However, in the above reaction process, the preparation of the catalyst is complicated and requires the introduction of precious metals, and the reaction temperature also needs to be above 700 °C to overcome the thermodynamic limitations of the reaction. Besides, the reverse water gas conversion reaction requires the consumption of hydrogen as the reducing agent, which has a methane-forming side reaction ($CO + 3H_2 \rightarrow CH_4 + H_2O$) and is able to hinder the improvement of CO selectivity.

The Boudouard reaction, as investigated by Huang et al. (2021), is a prevalent occurrence in the biomass gasification process. Governed by reaction kinetics and thermodynamics, the equilibrium shifts toward carbon monoxide (CO) generation only when the temperature surpasses 700 ℃ and the ΔG (change in Gibbs free energy) is negative (Chun and Song 2020). Research suggests that microwave-induced Boudouard reactions can alter the thermodynamics of the process, resulting in a reduction in the reaction's activation energy and a propensity for CO production (Bermúdez et al. 2014; Dai et al. 2021). Lahijani et al. (2015a, 2015b, 2015c) employed palm hollow fruit bundle ash as a catalyst to facilitate the reaction between oil palm shell biochar and CO_2, utilizing microwave energy at 900 ℃. The outcomes revealed a significant impact of microwaves in lowering the activation energy, leading to a 36% higher CO_2 conversion rate compared to conventional heating methods. Similarly, Dai et al. (2021) conducted a parallel study and observed that the CO_2 conversion rate with microwave heating exceeded 99% at 900 ℃, while traditional heating achieved a maximum CO_2 conversion of only about 29%. Kinetic calculations indicated that the activation energy required for the microwave-induced reaction was one-third of that necessary for conventional heating.

In the progression of a microwave reaction, the interplay between dielectric properties and microwaves is intricately connected. Effective absorbing materials play a pivotal role in minimizing the reflection of incident waves and enhancing the conversion of microwave energy into heat energy (Kappe 2004). The majority of material absorption property parameters are contingent on the incident microwave frequency, and modifying the frequency can enhance coupling with carbon materials, consequently achieving greater energy conversion efficiency (Ku et al. 2012). Balyan et al. (2023) employed a variable-frequency microwave reactor (5.85–6.65 GHz) to cleave C_2H_2, generating hydrogen and carbon nanotubes using a Ni-Pd bimetallic catalyst. The synergy between frequency and the catalyst manifested in a remarkable 100% conversion rate for C_2H_2 cleavage. In a similar vein, Hu et al. (2020) explored the synthesis of ammonia from nitrogen and argon using both a fixed-frequency microwave reactor (2450 MHz) and a variable-frequency microwave reactor (5850–6650 MHz). The variation in frequency significantly influenced the rate of product formation. Utilizing Ru/Al_2O_3 as the catalyst, the NH_3 generation rate reached 0.2 mmol g^{-1} cat h^{-1} at 6650 MHz frequency, contrasting with only 0.05 mmol g^{-1} cat h^{-1} at 2450 MHz frequency under equivalent conditions.

While significant research has been conducted regarding the microwave-enhanced Boudouard reaction, the impact of microwave frequency on this process remains unexplored in the current literature. Addressing this gap, this study aims to investigate the influence of microwave frequency on the Boudouard reaction. To achieve this, a variable frequency microwave reactor covering a range from 2430 to 6000 MHz was employed. Renewable biochar served as both the microwave absorbent and reactant. The examination of microwave frequency's effect on the Boudouard reaction was a focal point, leading to the optimization of related parameters. The investigation involved a comprehensive range of analyses, including N_2 adsorption, XRD, Raman, FT-IR, XPS, SEM, and vector network analysis, to characterize the changes in biochar's structure and microwave absorption properties

before and after reaction. Additionally, a comparison was drawn between the CO_2 conversion, CO selectivity, and CO production achieved using microwave and electric heating reactors. This work introduces a novel approach to utilizing variable-frequency microwaves to facilitate kinetically and thermodynamically constrained reactions externally.

2 Materials and methods

2.1 Materials

The biochar (coconut shell activated carbon) was sourced from Jiangsu Pushida Environmental Protection Technology Co., Ltd. The sample with a particle size of less than 0.4 mm was obtained after grinding and screening and was dried in an oven at 105 ℃ until its weight remained constant. Max Gases Limited provided the CO_2.

The pore structure analysis of the sample was conducted using the ASAP2020M automatic specific surface area and physical adsorption analyzer from Mackey Instruments, USA. Experimental parameters included N_2 adsorption and desorption at 77 K, followed by degassing at 150 ℃ for 6 h. Fourier infrared spectroscopy (Nicolet IS5, USA-Themo Field) was employed to analyze the structure and composition of the samples within a scanning wavenumber range of 400–4000 cm^{-1} and a resolution of 2 cm^{-1}. Additionally, the phase composition of the samples before and after the reaction was assessed using X-ray diffraction analysis (XRD, Nikaku SmartLab 9 KW), with a continuous scanning rate of 10°min^{-1} within the 2θ range of 5°–80°. Raman spectra was measured using Raman spectrometers (Horiba LabRAM HR Evolution, Japan). X-ray photoelectron spectroscopy (XPS, Thermo Scientific K-Alpha) was employed for full spectrum and narrow spectrum scanning to observe the elemental composition of the surface coating. Scanning electron microscopy (SEM, Zeiss Sigma500) and field emission transmission electron microscopy (TEM, Nippon Electron + JEM2100) were utilized to examine the microstructure of the samples before and after the reaction. The dielectric properties of biochar were analyzed using a vector network analyzer (VNA, Agilent PNA N5234A) with the coaxial method. The paraffin-material composite ratio was 7:3, and the inner and outer diameters of the sample ring were 7.00 mm and 3.04 mm, respectively. Gas products were examined using an Agilent 8890 gas chromatograph (Agilent Technologies, USA) equipped with a thermal conductivity detector (TCD), a hydrogen flame ionization detector (FID), a fill column (HayeSep Q), and a capillary column (HP-AL/M). The initial oven temperature was set at 50 °C and gradually increased to 120 °C at a rate of 10°min^{-1} over 7 min. The injector temperature was maintained at 200 ℃, while the TCD and FID detector temperatures were set at 200 ℃ and 250 ℃, respectively.

2.2 Reaction process

The experiment adopted a variable frequency microwave reaction device (Fig. 1), which mainly included a microwave continuous frequency modulation power supply, a microwave resonator, an infrared thermometer (200–1200 ℃), an infrared thermal imager (450–1800 ℃), a gas collection, and an analysis device. The microwave continuous frequency modulation power supply could continuously adjust the frequency within the range of 2430–6000 MHz with a 1 MHz difference, and the power could be varied from 0 to 500 W. The cavity took the form of a cylindrical resonator with dimensions of Φ 180*240 mm. Utilizing the thermal imager, the temperature distribution of the carbon layer beneath the reaction tube was directly observed through the germanium window. This approach enabled a direct assessment of the uniformity of the temperature distribution across the carbon layer during microwave irradiation.

The experiment involved packing a quartz tube, 8 mm in inner diameter, with quartz cotton. Following this, 1 g of biochar was meticulously placed into the quartz tube and secured using additional quartz cotton. The quartz tube was linked to the microwave reaction system, and N_2 or Ar was passed into the reactor to sustain an inert atmosphere. The temperature variations of the reaction bed were continuously monitored in real-time by the infrared thermometer and thermal imager. Post-reaction, the gas was collected in gas sampling bags for subsequent offline analysis using gas chromatography.

The electric-heated fixed bed reactor (FB) was operated under identical reaction conditions. The fixed-bed tube furnace was gradually heated, maintaining a steady heating rate of 10°min^{-1} until the predetermined temperature was achieved. The entire system underwent thorough purging with quantitative N_2, and the device's air tightness was verified. The product gas was collected using an aluminum foil collection bag and subsequently introduced into the gas chromatography for qualitative and quantitative analyses.

2.3 Data evaluation

The CO_2 conversion is calculated based on the volume fraction of the exported product (Menéndez et al. 2007).

$$\eta_{CO_2} = \frac{0.5X_{CO}}{X_{CO_2}+O.5X_{CO}} \times 100\%, \quad (1)$$

where η_{CO_2} is CO_2 conversion rate, %; X_{CO_2}, X_{CO} are the volume fractions of CO_2 and CO in the outlet gas which were measured as a percentage (%).

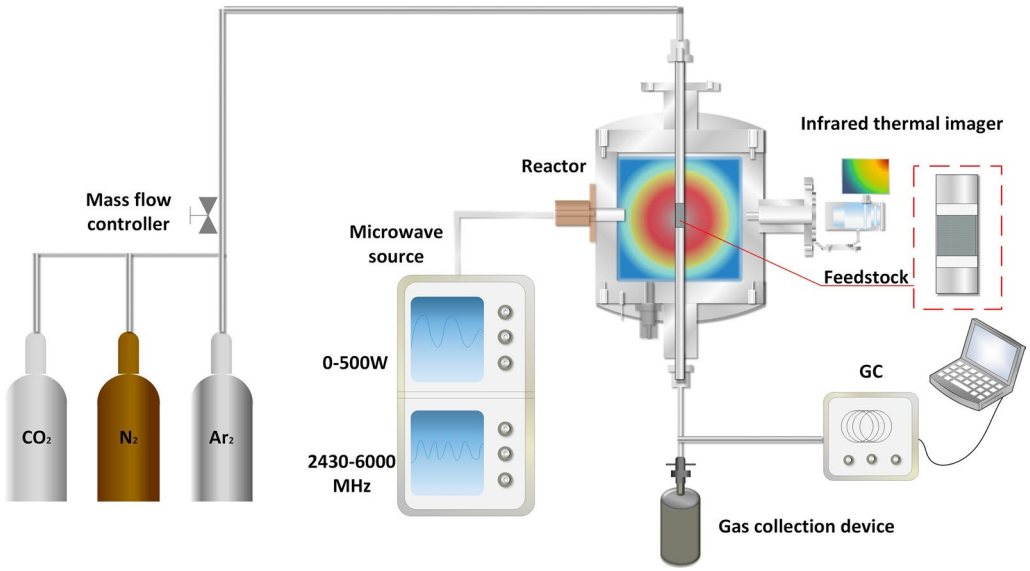

Fig. 1 Schematic of variable frequency microwave assisted fixed-bed reactor

The selectivity of CO is calculated by the following formula.

$$S_{CO} = \frac{X_{CO}}{X_{H_2}+X_{CO}} \times 100\%, \quad (2)$$

where X_{H_2}, X_{CO} is the volume fractions of H_2 and CO in the outlet gas which were measured as a percentage (%).

The CO production E_{CO} is the amount of CO (in μmol) that can be produced per kJ of energy.

$$E_{CO} = \frac{v_{CO_2} \times h \times S_{CO} \times \eta_{CO_2}}{energy\ input} \times 100\%, \quad (3)$$

where η_{CO_2} is CO_2 conversion rate, %; v_{CO_2} is CO_2 flow, ml min^{-1}; S_{CO} is CO selectivity, %; h is reaction time, min.

3 Results and discussion

3.1 The influence of microwave frequency on CO_2 conversion

The conversion of microwave energy into heat hinges on the dielectric properties of the absorbing material, a factor profoundly impacted by the microwave frequency (Thostenson and Chou 1999). To investigate the influence of microwave frequency on the Boudouard reaction, a variable-frequency microwave reactor was employed, with operating frequencies set at 2450, 2750, 2760, 4225, 4405, and 5225 MHz, while maintaining a constant microwave power of 100 W.

As depicted in Fig. 2a, discernible variations in CO_2 conversion are evident across different microwave input frequencies. Under the conventional microwave frequency of 2450 MHz, where the temperature of the carbon layer was 323°C, the Boudouard reaction failed to occur. Maintaining a constant power level, the trend in CO_2 conversion demonstrated an initial increase followed by a subsequent decrease as the frequency rose from 2450 to 5525 MHz. Notably, at the frequency of 4225 MHz, the CO_2 conversion reached its zenith, registering at 8.8%. The CO_2 conversion rates at frequencies of 2750, 2760, 4405, and 5225 MHz were 4.5%, 5.6%, 4.3%, and 3.9%, respectively. The impact of frequency variations on CO selectivity was relatively modest, fluctuating between 94.3% and 100%. It is noteworthy that at the frequency of 4225 MHz, the CO selectivity reached its maximum value of 100%.

The adjustment in frequency induced changes in the electromagnetic field, consequently influencing the temperature distribution within the system. The temperature elevation curves for various frequencies are illustrated in Fig. 2b. As expected, the temperature transitioned from 537.7 °C to 570.4 °C as the microwave frequency increased from 2760 to 4225 MHz. At a microwave frequency of 5225 MHz, suboptimal heating was observed, peaking at 454.7 °C, with a heating rate of 0.9 ℃ min^{-1}. In contrast, the heating rates for 2760 MHz and 4225 MHz were 17.5 ℃ min^{-1} and 24.1 ℃ min^{-1}, respectively. This observation underscores that at 4225 MHz, the biochar exhibited enhanced microwave coupling, enabling efficient conversion of microwave energy into heat energy and thereby fortifying the reaction.

The gas yield per unit of energy is a key parameter for achieving efficient energy conversion. Maximizing product yield per unit of energy through optimizing reaction conditions is crucial for reducing economic costs and

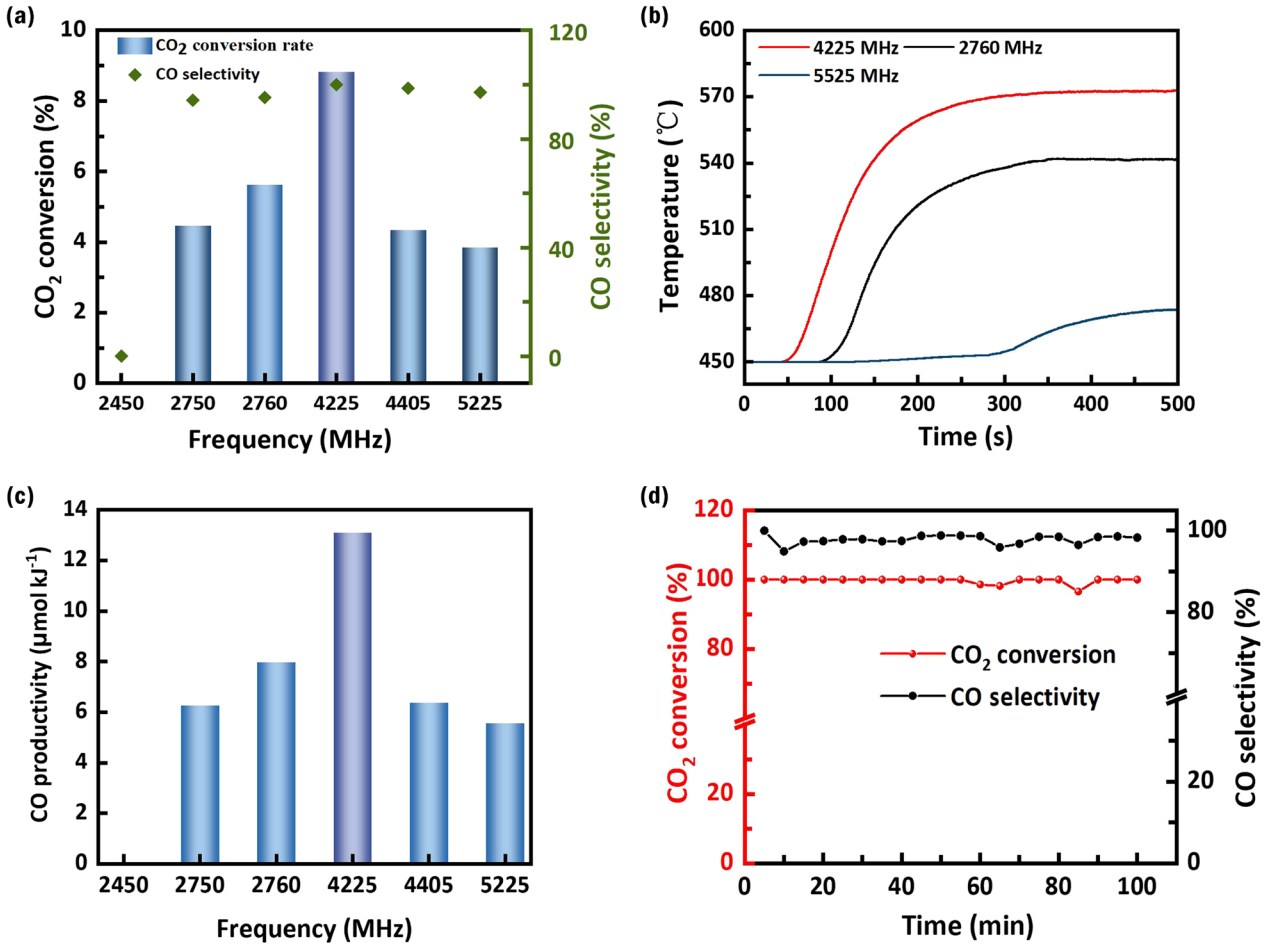

Fig. 2 **a** The CO_2 conversion and CO selectivity at different microwave frequencies (100 W, 5 min). **b** Temperature curves for 500 s at different frequencies. **c** The CO production at different frequencies (100 W, per kJ energy). **d** CO_2 conversion and CO selectivity with the reaction time of 100min (275 W, 796 ℃)

decreasing reliance on energy resources. To investigate the relationship between energy consumption and CO yield at different frequencies, we analyzed the μmol of CO produced per kilojoule of energy at various microwave frequencies, introducing the E_{CO} to describe this metric, as detailed in Fig. 2c. The results indicate that, as the frequency increased from 2450 to 5225 MHz, E_{CO} exhibited an initial increase followed by a subsequent decrease. At the frequency of 4225 MHz, E_{CO} reached its maximum, producing 13.1 μmol of CO per kJ of energy consumed. However, as the frequency increased to 5225 MHz, the amount of CO produced per kJ of energy consumed decreased to 5.6 μmol. This further highlights the unique advantage of the 4225 MHz frequency in achieving low energy consumption and high-efficiency conversion.

A carbon stability evaluation was conducted, and the results are presented in Fig. 2d. With an increase in reaction time, the CO_2 conversion remained consistently close to the initial conversion of 100%, exhibiting minor fluctuations. The main gas component was CO, with an initial selectivity of 100%. As trace volatiles were analyzed out of the biochar, the selectivity fluctuated slightly but consistently remained above 97.0%. Approximately 3.0% of H_2 was attributed to the pyrolysis of the carbon material itself. The involvement of biochar in the reaction, acting as an absorber, imparts a certain influence on microwave absorption during the progression of the reaction.

The Boudouard reaction process, illustrated in Fig. 3, commences by transferring oxygen to the surface, oxidizing one of the active sites, and releasing CO. The electric field vector generated by the incoming microwave induces the formation of momentary electron–hole pairs, recognized as the anions and cations during the chemical reaction. These pairs likely favor carbon and oxygen in CO_2, enhancing the oxidation process at the active

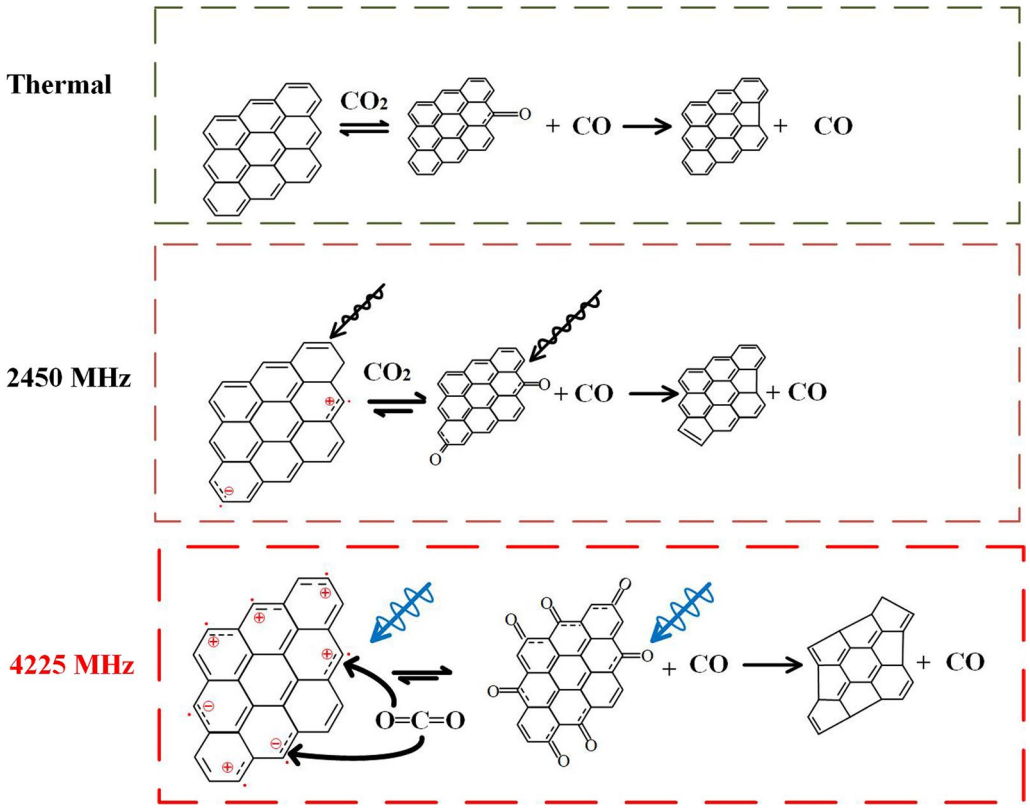

Fig. 3 Underlying mechanism responsible for the distinct influence of microwave frequency on Boudouard reaction

site. Following oxidation, polar functional groups on the carbon surface couple with the microwave through the Debye relaxation process, selectively heating the polar sites of carbon and expediting the desorption of CO from the carbon surface (Hunt et al. 2013). According to Suttisawat et al. (2012), microwaves confer an advantage in enhancing the separation between products and catalyst surfaces, thereby improving reaction efficiency.

Moreover, distinct microwave absorption capacities of the catalyst and reactants create notable temperature gradients between them, contributing to enhanced reaction rates (Horikoshi et al. 2014). Activated carbon, as a porous matrix, forms a heterogeneous phase reaction system with the reaction gas. The difference in microwave absorption efficiency leads to varying temperature distributions during microwave irradiation, becoming the driving force for molecular desorption and mass transfer from the surface of activated carbon (Horikoshi and Serpone 2014).

The presence of hotspots, amplifying chemical reactions, was discovered by Tsukahara et al. (2010). Horikoshi et al. (2013) suggested that using microwaves at 5.8 GHz, rather than 2.45 GHz, positively impacted reactions in a microwave-assisted system. Microwave-induced effects, such as enhanced reaction rates, increased yields, and directed reaction selectivity, can be attributed to the distinct heating patterns generated by the interaction of oscillating electric and magnetic fields with substances in the reaction system (Tsukahara et al. 2010). Altering the incident microwave frequency leads to changes in the electromagnetic field, significantly affecting the mass transfer process and the occurrence of "hot spots," ultimately influencing the chemical reaction.

In this study, the highest CO_2 conversion observed at 4225 MHz can be attributed to several factors. Firstly, efficient coupling between the electromagnetic field distribution and biochar at this specific microwave frequency resulted in a high biochar temperature and rapid heating rate, facilitating the highly endothermic Boudouard reaction toward CO generation. Secondly, at this frequency, the distribution of the microwave's electromagnetic field promoted the cleavage of chemical bonds within CO_2 and enhanced the exposure of active sites on the biochar surface. Consequently, both the CO_2 conversion rate and CO production were significantly increased. Thirdly, microwave frequency had a considerable impact on the occurrence of "hot spots" within the microwave

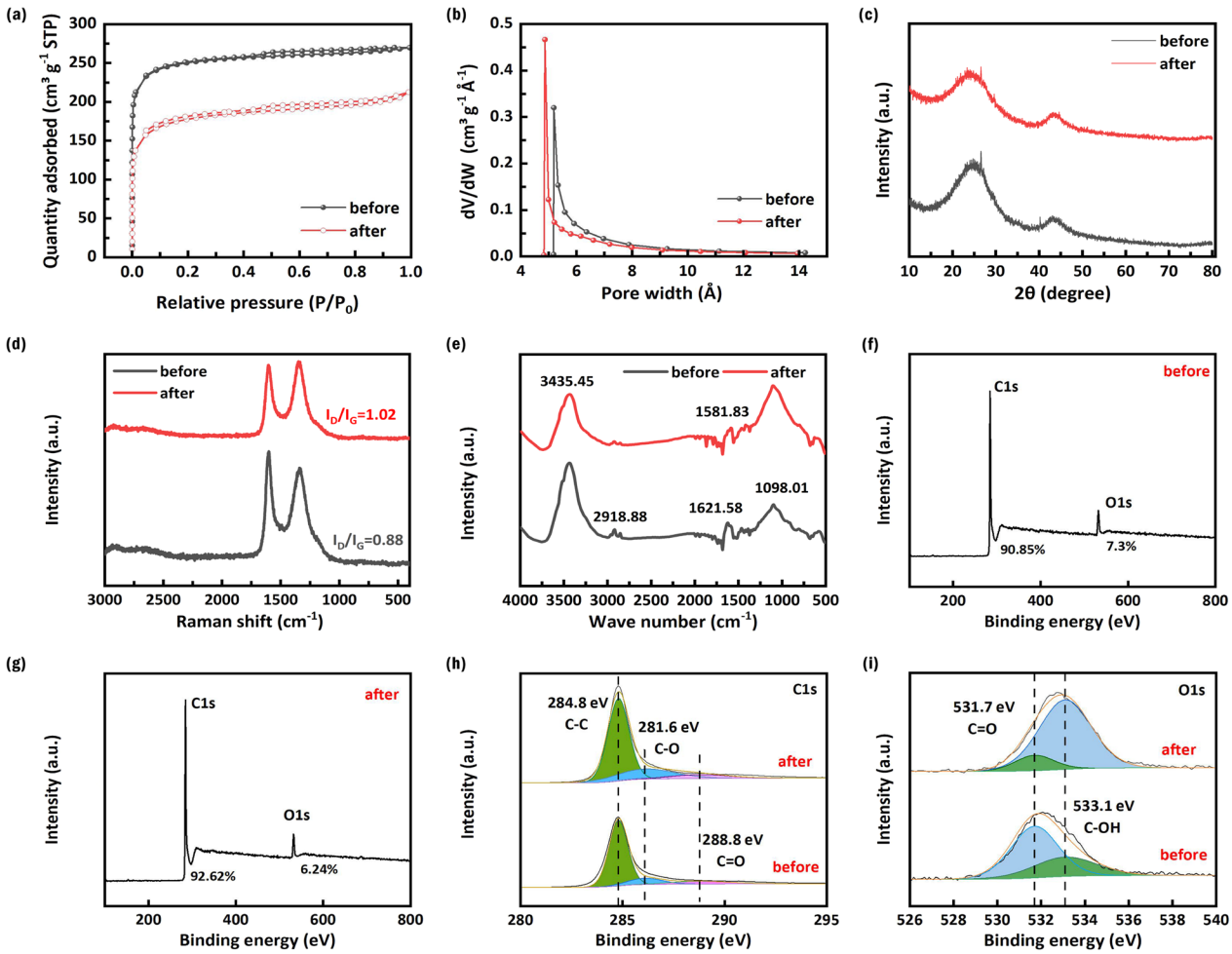

Fig. 4 Illustration of various analyses performed on the biochar (**a**) N_2 adsorption–desorption isotherm, (**b**) Pore size distributions, (**c**) XRD patterns, (**d**) Raman spectra, (**e**) FT-IR spectra, (**f**–**i**) XPS survey spectra and high-resolution C1s and O1s

field, a phenomenon known to intensify the chemical reaction.

3.2 Characterization of biochar

3.2.1 Morphological structure of biochar

The pore structure analysis of biochar before and after the reaction (at 4225 MHz, 275 W, 100 min) was conducted using N_2 adsorption–desorption isotherms. It was observed that both adsorption isotherms (Fig. 4a) followed a typical type I isotherm pattern (Bläker et al. 2019). At low relative pressures, the gas rapidly filled the microporous region, causing the adsorption curve to increase exponentially. The hysteresis phenomenon indicated that there were mesoporous in addition to micropores in biochar (Yuan et al. 2020). Before the reaction, the biochar exhibited a specific surface area (S_{BET}) of 858 $m^2\ g^{-1}$(Additional file 1: Table S1), with an average pore size of 19.5 Å. The S_{BET} of the micropores contributed to 825 $m^2\ g^{-1}$. After the reaction, the S_{BET} of the biochar decreased to 622 $m^2\ g^{-1}$, while the average pore size increased to 21.3 Å. The main pore size distribution of fresh biochar (Fig. 4b) was around 5.2 Å, and the pore size of the biochar after the reaction was mainly around 4.9 Å, both of which were mainly composed of micropores. Micropores would act as the dihedral angle of microwave reflection, and the microwave was reflected between the dihedral angles, extending its propagation path in the absorbing medium, and resulting in the loss of electromagnetic energy (Wu et al. 2018). Furthermore, the porous structure provided more active sites for chemical reactions and increased gas diffusion channels, consequently enhancing the overall reaction rate (Lahijani et al. 2015a, b, c; Zhang et al. 2019; Ahmad et al. 2020).

The XRD results of biochar are shown in Fig. 4c. The biochar before and after the reaction had two diffraction peaks near 24.7° and 43.2° on the graphitic carbon (002) and (100) crystal planes, indicating that the biochar

before and after the reaction existed in the form of amorphous carbon. Compared with the peak of fresh biochar, the diffraction peak height of the sample after reaction was reduced, and the slit width was increased, indicating that the degree of graphitization of biochar after reaction was reduced. The Raman shift map also illustrated this change (Fig. 4d). Both pre-reaction and post-reaction biochar exhibited a D peak at 1350 cm^{-1} and a G peak at 1580 cm^{-1} in their Raman spectra. After the reaction, the biochar tended towards disorder, as evidenced by the I_D/I_G values of 0.88 and 1.02 before and after the reaction, respectively.

The dielectric properties of a material are also influenced by the presence of functional groups. We utilized a Fourier infrared spectrometer to analyze the material. It was observed that the characteristic infrared absorption peaks of the initial biochar were primarily at 3435.45, 2918.88, 1621.58 and 1098.01 cm^{-1} (Fig. 4e), respectively, while the peaks of the biochar after the reaction shifted from 1621.58 cm^{-1} to 1581.83 cm^{-1}. The peak at 3435.45 cm^{-1} mainly corresponds to hydroxyl group stretching vibrations. Peak at 2918.88 cm^{-1} is the absorption peak of C-H bonds. Peaks at 1581.83 and 1621.58 cm^{-1} are generally associated with C=O and C=C stretching vibrations. Peak at 1098.01 cm^{-1} usually includes the absorption peaks of C–O, phenol-based C–OH, and C–C bonds (Marco and Kleber 2010). The defect position and unsaturated bonds on the material's surface can be considered dipoles, and the coupling of microwaves and dipoles enhances the material's capacity for microwave loss and absorption (Wang et al. 2008; Ma et al. 2016a, b).

X-ray photoelectron spectroscopy (XPS) was employed to investigate the chemical composition of the biochar. The XPS survey spectra are illustrated in Fig. 4f–i. According to XPS calculations, the C and O were calculated to be 90.9% and 7.3% of fresh biochar, while the C and O contents of biochar after the reaction were 92.6% and 6.2%, respectively. The high-resolution C1s spectra displayed in Fig. 3h revealed distinct peaks of C–C (284.8 eV), C–O (281.6 eV), and C=O (288.8 eV) present in both the pre-reaction and post-reaction biochar. Illustrated by the high-resolution O1s spectra in Fig. 3i, both pre-reaction and post-reaction biochar showcased peaks corresponding to C=O (531.7 eV) and C–OH (533.1 eV). Nevertheless, in comparison to the post-reaction biochar, the C=O peak was less prominent in the pre-reaction biochar, while the content of C–OH was more pronounced.

The SEM images were used to observe the appearance of biochar (Fig. 5). It can be clearly seen that the biochar before and after the reaction had a honeycomb 3D skeleton structure, developed pores, and irregular pores are densely arranged. Holes and the air layer inside holes are considered wave-absorbing "composite materials" because of their different dielectric properties. The carbon medium with a porous structure will form a rich carbon-air interface inside. When the incident electromagnetic wave reaches the gas–solid phase interface, a large amount of charge will accumulate at the interface, causing strong space charge polarization, which is one of the paths of electromagnetic wave attenuation, and interface polarization (Ma et al. 2016a, b).

3.2.2 Microwave absorption properties

The heating rate and temperature distribution of materials under microwave irradiation depend on their

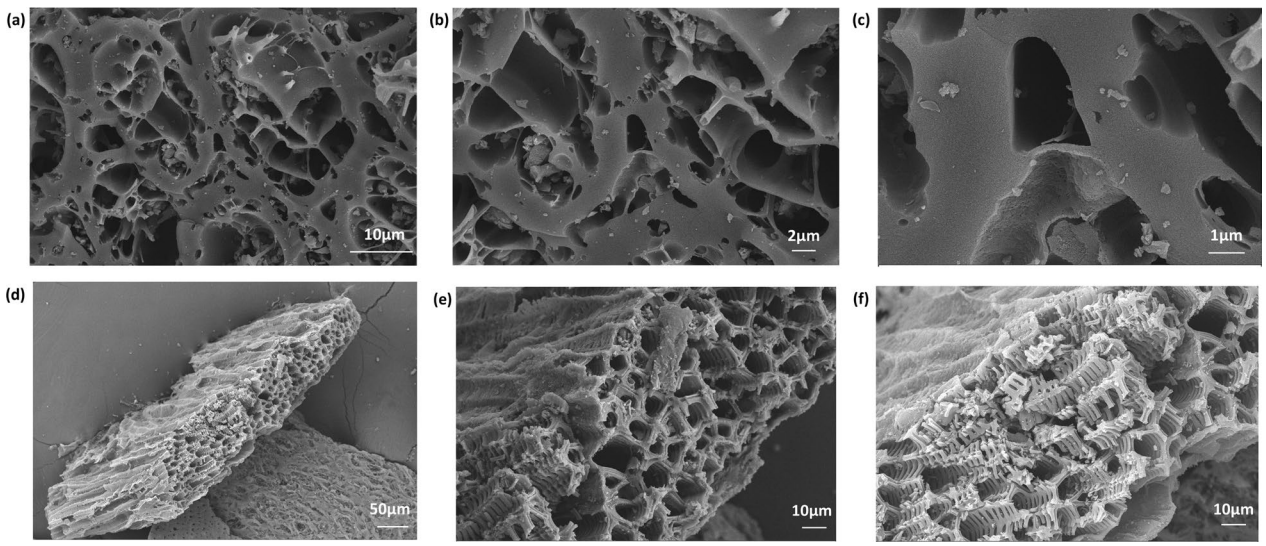

Fig. 5 SEM image of the biochar (**a**-**c**) before and **d**-**f** after the reaction

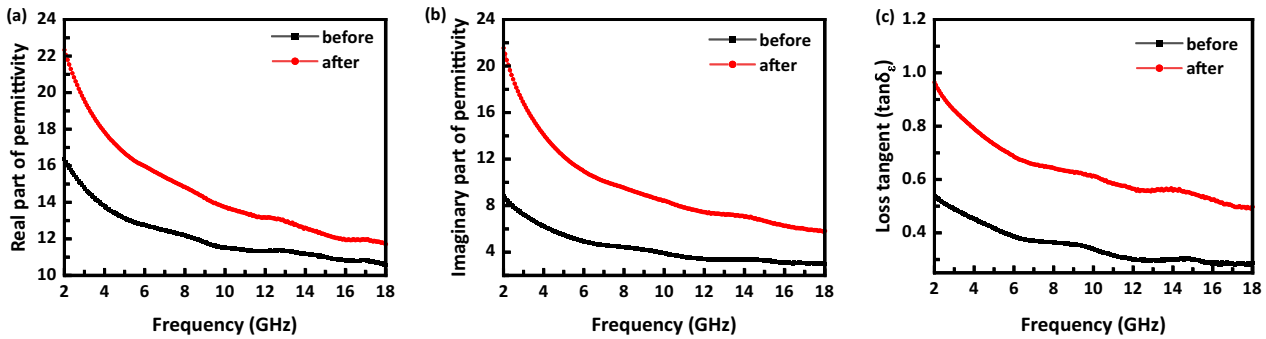

Fig. 6 Complex dielectric constant of biochar in the range of 2–18 GHz. **a** Real part of permittivity, **b** imaginary part of permittivity, and **c** loss tangent.

dielectric properties, which can be influenced by factors such as material type, preparation process, and microwave frequency (Garcia-Banos et al. 2019). Biochar underwent characterization using a vector network analyzer, revealing changes in its dielectric properties in response to fluctuations in microwave frequency.

As illustrated in Fig. 6a, b, the dielectric constant of biochar exhibited a decline with increasing microwave frequency. Notably, the amplitude of the decrease was more pronounced within the range of 2–5 GHz. When the frequency was 5 GHz, the ε' of fresh biochar was 13.1 and the ε'' was 5.5. The ε' and ε'' of biochar after reaction were 16.7 and 12.2, respectively. The permittivity of the biochar after the reaction was higher than that of the fresh biochar. The permittivity of fresh biochar varied from 10.6 to 16.4 in the real part and from 3.0 to 8.8 in the imaginary part, while that of the biochar after the reaction varied from 11.7 to 22.3 in the real part and from 5.8 to 21.6 in the imaginary part, which proved that the biochar after the reaction had better microwave absorption capacity. The biochar after the reaction had advantages in charge storage and dissipation.

The dielectric losses of both the biochar before and after the reaction exhibit a gradual decrease as the frequency increases, with the maximum dielectric tangent values ($tan\delta\varepsilon$) peaking around 2 GHz. For the biochar before the reaction and the biochar after the reaction, these values were 0.5 and 1.0, respectively (Fig. 6c). As the microwave frequency increased from 2 to 6 GHz, the $tan\delta\varepsilon$ values of the biochar before and after the reaction gradually decreased to 0.4 and 0.7, respectively. Within the frequency ranged of 6 to 12 GHz and 12 to 18 GHz, the $tan\delta\varepsilon$ values of the biochar before and after the reaction first increased and then decreased. The $tan\delta\varepsilon$ value of the biochar before the reaction remained below 0.4, while the $tan\delta\varepsilon$ value of the biochar after the reaction remained below 0.7. An elevated dielectric loss tangent value indicates a greater dielectric loss capacity. However, such an elevated value may result in inadequate impedance matching, leading to multiple microwaves being reflected from the sample surface. Consequently, this scenario can lead to insufficient microwave absorption (Jia et al. 2018). Post-reaction biochar exhibits an enhanced dielectric loss capacity, making it an efficient microwave absorber.

3.3 Optimization study

3.3.1 The influence of heating method

To investigate the impact of different heating methods on the reaction and elucidate the underlying mechanism of microwave heating, the Boudouard reaction was carried out in two types of reactors: a microwave reactor (MW) and an electrically heated fixed bed reactor (FB). By adjusting the microwave frequency and power, the temperature within the MW was regulated while maintaining temperature consistency between the two reactors. The volume space velocity of CO_2 was set at 239 h^{-1}, and the reaction time was 5 min.

The CO_2 conversion under the two heating methods is shown in Fig. 7a. During the whole period of heating, the CO_2 conversion of MW was always higher than that of the FB, and such difference greatly increased as the temperature of reaction rose. Given the reaction's notably endothermic nature, CO_2 conversion remained below 50% when the temperature remained below 700 ℃. Upon reaching 796 ℃, the conversion rate under electric heating was 3.6%, while microwave heating achieved a 100% conversion rate, signifying an increase of 96.4%. Different from the obvious increase in CO_2 conversion, the difference in CO selectivity between the two heating methods was not obvious (Fig. 7b). In the electric heating reactor, the selectivity of CO was maintained at 100%, and the selectivity of CO decreased to 90.7% when the temperature reached 796 ℃. Conversely, in the microwave reactor, CO selectivity exhibited a slight reduction as temperature increased, and the CO selectivity was 100% at 796 ℃.

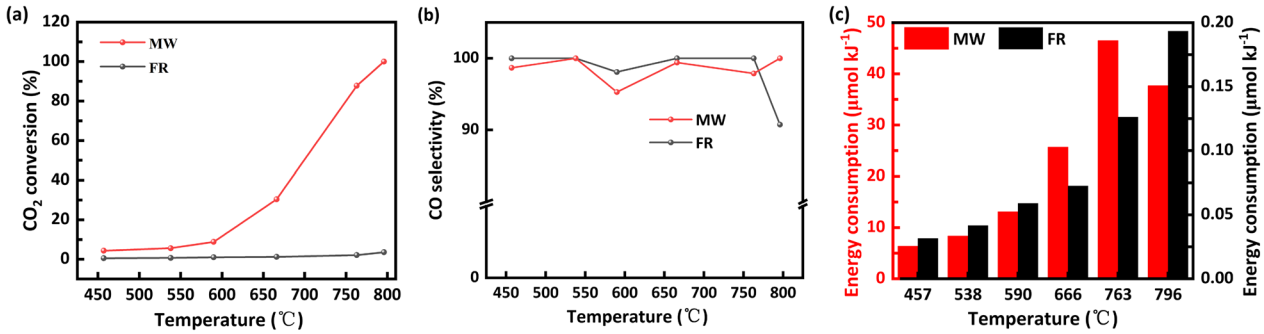

Fig. 7 Illustration of the reaction results in the MW and FR heating setups: (**a**) conversion of CO_2 (**b**) selectivity of CO (**c**) CO production (per kJ energy)

In addition, we also evaluated the E_{CO} of two heating methods, and across the entire temperature range, microwave reactions exhibited superior energy efficiency compared to electric heating. The CO production per kJ energy (E_{CO}) of the two heating methods was shown in Fig. 7c. At 457 ℃, the E_{CO} of electric heating was 0.03 μmol kJ^{-1}, while that of the microwave was 6.37 μmol kJ^{-1}. This phenomenon persisted as the temperature increased. When the temperature approached 600 °C, the microwave-induced CO production remained ~ 218 times higher compared to electric heating. With the increase in reaction temperature, both CO_2 conversion and CO production significantly rose, indicating a substantial reduction in energy consumption due to the increased conversion rate.

In the traditional electric heating process, energy is conveyed to the substance via mechanisms like convection, conduction, and thermal radiation, driven by temperature gradients. In contrast, microwave energy directly interacts with molecules and electromagnetic fields within the material, leading to the conversion of electromagnetic energy into heat energy (Lam et al. 2012). According to research (Hunt et al. 2013), the apparent enthalpy of reactions induced by microwaves was notably lower in comparison to electrothermal reactions, as assessed through the standard heat of formation. The change was caused by microwaves injecting extra energy into the carbon. Microwaves interacted with carbon not only as a source of selective heating but also as an energetics of a different rate-determining process at the carbon surface. The enhancement of the microwave reaction to Boudouard stemmed from a distinct unique space-charge polarization mechanism between the microwave and the carbon material.

3.3.2 The influence of microwave power

The Boudouard reaction exhibits a strongly endothermic nature, and although microwave radiation can reduce the reaction temperature to some extent, high temperatures are still required to maintain a high CO_2 conversion. With the microwave transmission frequency kept at 4225 MHz, we further increased the power to explore its effect on the CO_2 conversion which is shown in Fig. 8a. As the power input escalated, both temperature and CO_2 conversion exhibited an upward trajectory. At 100 W power, the CO_2 conversion rate was 8.8%. Upon elevating the power to 250 W, the conversion rate surged to 87.8%. Further increasing the power resulted in a relatively stable conversion rate. The highest conversion rate of 100% was achieved at 275 W, with a corresponding temperature of 796 ℃. The temperature rise curves of 100 W and 275 W are shown in Fig. 8b. The increase of power not only substantially raised the average temperature within the reaction bed but also greatly increased the temperature rise rate. The temperature rise rate of 100 W was 34.7 ℃ min^{-1}, while it was 107.4 ℃ min^{-1} at the power of 275 W. The influence of power on CO selectivity is relatively minimal, manifesting only a slight decrease with increasing power, but the decreasing trend is not significant. At a power of 275 W, CO selectivity reached 100%.

3.3.3 The influence of carrier gas

The effects of different carrier gases (N_2/Ar) on the Boudouard reaction within the variable frequency microwave reactor were investigated, and the findings are illustrated in Fig. 8c. The CO_2 conversion was different with different carrier gases. Introducing N_2 and Ar elevated the CO_2 conversion rate by 22.2% and 25.9%, respectively. Recent studies (Snoeckx et al. 2013; Tiwari et al. 2019) have revealed that selective heating of the interface between the catalyst's active site and the reaction intermediate by microwaves lead to the activation of stable molecules, such as N_2 and CH_4, by coupling microwave radiation in the solid with dipoles through a relaxation process, thus increasing the reaction rate and conversion. Lahijani et al. (2015a, b, c) observed that during the carbon-CO_2

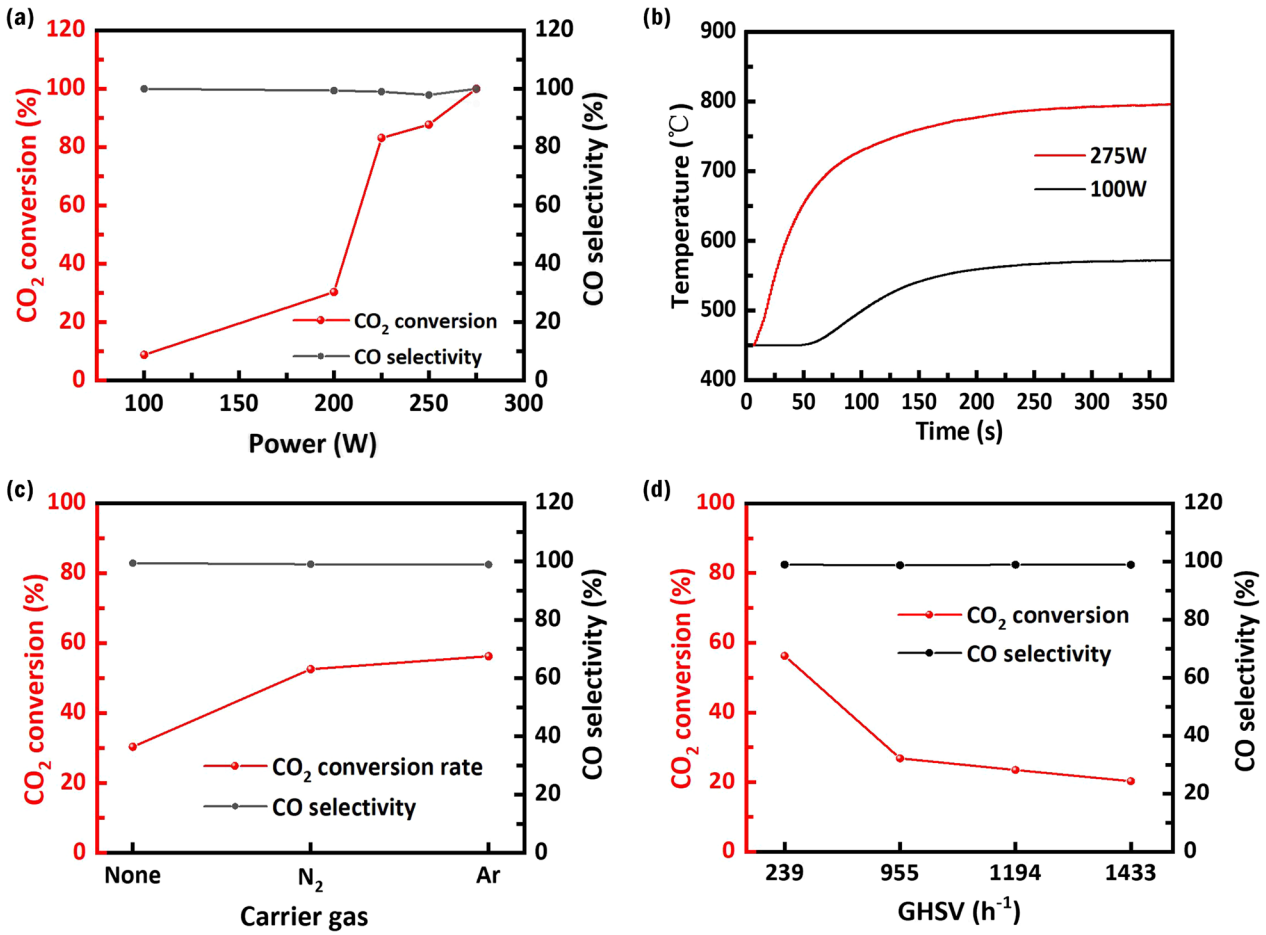

Fig. 8 **a** CO_2 conversion and CO selectivity at different power. **b** Temperature curves for 500 s at different power. **c** CO_2 conversion and CO selectivity of different carrier gases, and **d** CO_2 conversion and CO selectivity of different GHSV

reaction, the mixture of multiple gases altered the partial pressure of CO_2. Pressure, acting as a driving force for gas-phase reactions, influenced the diffusion rate of reactants into carbon pores and the reaction rate of the pore-diffusion-controlled reaction system. These variations led to differences in the product's CO concentration. Therefore, filling the microwave reactor with an appropriate inert gas favored the progression of the Boudouard reaction, although it did not significantly affect gas selectivity, with the selectivity of CO remaining stable at 99%.

It has been discovered that microwave exposure to certain semiconductor materials or carbon-based materials can induce microwave discharge, leading to the formation of microwave plasma. Menendez et al. (2011) provided image evidence for the formation of plasma when carbon was subjected to microwave heating. Two types of plasma were observed within the temperature range of 400 ℃ and 400–700 ℃, respectively. They found that the temperature in the plasma region increased more rapidly compared to the surrounding areas. Upon exposure to heat, external electric fields, or radiation, gas atoms or molecules undergo excitation and ionization. Subsequently, the resultant high-energy free electrons collide with these atoms or molecules, expediting the fragmentation of chemical bonds. This phenomenon facilitates the occurrence of chemical reactions, leading to increased ease of reaction initiation, reduced energy consumption, and heightened selectivity (Sun et al. 2016). Specific electrode structures are more prone to breakdown in media with low dielectric strength (Sun et al. 2016). Ar has a dielectric strength of 0.2 MV m^{-1}, while N_2 has a dielectric strength of 0.9 MV m^{-1}. Chen et al. (2012) found that the discharge frequency of Cu and SiC particles under microwave irradiation was lower in an N_2 atmosphere compared to an Ar atmosphere. Therefore, incorporating a certain proportion of Ar is crucial for promoting the microwave heating process and chemical reactions.

3.3.4 The influence of GHSV

The gas hourly space velocity (GHSV) is commonly considered one of the key parameters in gas–solid reactions, indicating the duration the gas spends within the catalytic system. This extended contact time between the gas and the catalyst promotes a more comprehensive progression of the reaction. In the variable frequency microwave reactor, Ar was employed as the carrier gas to examine the influence of GHSV on the Boudouard reaction. Figure 8d displays the CO selectivity and CO_2 conversion rate. An increase in GHSV lead to a reduction in the conversion rate, which decreased sharply from 56.3% to 26.8% as the space velocity rose from 239 h^{-1} to 955 h^{-1}. Upon further elevation to 1433 h^{-1}, the conversion rate dropped to 20.3%, with the decreasing trend slowing down. Excessively high gas flow rates significantly increased heat dissipation, lowering the temperature of the carbon layer, and shortening the gas residence time, thereby decreasing the conversion rate. Product selectivity was less impacted by the air velocity, with the selectivity of CO consistently maintained around 98.9%.

4 Conclusion

This study delved into the impact of microwave frequency on the Boudouard reaction using a variable-frequency microwave reactor. The aim was to discover a method for achieving efficient and low-energy CO_2 conversion. We compared the distinct advantages of microwave heating. Under temperature conditions of 796 ℃, microwave heating enhanced CO_2 conversion by 96.4% compared to electric heating, with a corresponding increase of 37.5 μmol kJ^{-1} in CO production. At a low power of 100W, there was no reaction under the conventional microwave frequency of 2450 MHz, in contrast, we achieved CO_2 conversion at a specific frequency of 4225 MHz, with a conversion rate of 8.8%. Under optimized reaction conditions, specifically, a frequency of 4225 MHz and a power of 275 W, CO_2 conversion reached 100%, sustained for over 100 min. The study further explored the structural and performance changes in fresh and reacted biochar. After the reaction, both the real and imaginary components of the dielectric constant of the reacted biochar increased, accompanied by a significant rise in the tangent of the dielectric loss angle. These findings indicate that reacted biochar possesses enhanced capacity for charge storage and consumption, with an amplified potential to convert microwave energy into thermal energy after the reaction. In summary, precise control of microwave frequency holds significant importance for achieving efficient and low-energy reaction processes.

Supplementary Information

The online version contains supplementary material available at https://doi.org/10.1007/s42773-023-00297-9.

Additional file 1: Figure S1. H_2 selectivity: (a) different heating methods, (b) different heating methods, (c) different microwave power, (d) different carrier gas, (e) different GHSV, (f). Carbon stability test. **Figure S2**. TEM mapping of biochar before(a-c) and after(d-f) the reaction. **Table S1**. Specific surface area and pore structure parameters of biochar.

Acknowledgements
The author would like to acknowledge Jiangsu Pusta Environmental Protection Technology Co., Ltd. for providing us with biochar.

Author contributions
All authors contributed to the conception and design of the study. JR completed materials preparation, experimental investigation, data collection, and analysis. The first draft of the manuscript was written by JR, and the experimental supervision, manuscript review and revision were completed by JW. Conceptualization, funding acquisition, resources, supervision, and review are the contributions of supervisor JJ. XY completed method guidance. Project support and experimental raw materials came from AW. All authors have commented on previous manuscript editions. All authors read and approved the final manuscript.

Funding
This work was supported by the Special funds for basic scientific research in Chinese Academy of Forestry (Grant No. CAFYBB2020ZF001), and National Natural Science Foundation of China (Grant No. 52376195).

Data availability
The datasets used or analyzed during the current study are available from the corresponding author on reasonable request.

Declarations

Competing interests
The authors have no relevant financial or non-financial interests to disclose. The authors declare that they have no known competing financial interests or personal relationships that could have appeared to influence the work reported in this paper.

Author details
[1]Institute of Chemical Industry of Forest Products, Chinese Academy of Forestry (CAF), No. 16, Suojin Five Village, Nanjing 210042, China. [2]Jiangsu Coo-Innovation Center for Efficient Processing and Utilization of Forest Resources, College of Chemical Engineering, Nanjing Forestry University, Longpan Road 159, Nanjing 210037, China. [3]Key Laboratory of Energy Thermal Conversion and Control of Ministry of Education, School of Energy and Environment, Southeast University, Nanjing 210096, China.

Received: 9 September 2023 Revised: 16 December 2023 Accepted: 23 December 2023
Published online: 04 March 2024

References

Ahmad J, Vakalis S, Patuzzi F, Baratieri M (2020) Effect of process conditions on the surface properties of biomass chars produced by means of pyrolysis and CO_2 gasification. Energy Environ 32(8):1378–1396. https://doi.org/10.1177/0958305X20948237

Jensen LIA, Blomberg S, Hulteberg C (2021) Effect of Pd and Ir as promoters in the activity of Ni/$CeZrO_2$ catalyst for the reverse water-gas shift reaction. Catalysts 11(9):1076. https://doi.org/10.3390/catal11091076

Bai S, Shao Q, Wang P, Dai Q, Wang X, Huang X (2017) Highly active and selective hydrogenation of CO_2 to ethanol by ordered Pd-Cu nanoparticles. J Am Chem Soc 139(20):6827–6830. https://doi.org/10.1021/jacs.7b03101

Balyan S, Jiang C, Caiola A, Hu J (2023) Microwave catalytic conversion of acetylene for co-production of hydrogen and carbon nanotubes. Chem Eng J 454:140115. https://doi.org/10.1016/j.cej.2022.140115

Bermúdez JM, Ruisánchez E, Arenillas A, Moreno AH, Menéndez JA (2014) New concept for energy storage: microwave-induced carbon gasification with CO_2. Energy Convers Manage 78:559–564. https://doi.org/10.1016/j.enconman.2013.11.021

Bläker C, Muthmann J, Pasel C, Bathen D (2019) Characterization of activated carbon adsorbents—state of the art and novel approaches. Chem Bio Eng Reviews 6(4):119–138. https://doi.org/10.1002/cben.201900008

Chan YH, SyedAbdulRahman SNF, Lahuri HM, Khalid A (2021) Recent progress on CO-rich syngas production via CO_2 gasification of various wastes: a critical review on efficiency, challenges and outlook. Environ Pollut 278:116843. https://doi.org/10.1016/j.envpol.2021.116843

Chen W, Gutmann B, Kappe CO (2012) Characterization of microwave-induced electric discharge phenomena in metal-solvent mixtures. ChemistryOpen 1(1):39–48. https://doi.org/10.1002/open.201100013

Chun YN, Song HG (2020) Microwave-induced carbon-CO_2 gasification for energy conversion. Energy 190:116386. https://doi.org/10.1016/j.energy.2019.116386

Dai H, Zhao H, Chen S, Jiang B (2021) A microwave-assisted boudouard reaction: a highly effective reduction of the greenhouse gas CO_2 to useful CO feedstock with semi-coke. Molecules 26(6):1507. https://doi.org/10.3390/molecules26061507

Fu H, Liu X, Wu Y, Zhang Q, Wang Z, Zheng Z, Cheng H, Liu Y, Dai Y, Huang B, Wang P (2023) Construction of a bismuth-based perovskite direct Z-scheme heterojunction Au-Cs3Bi2Br 9/V_2O_5 for efficient photocatalytic CO_2 reduction. Appl Surf Sci 622:156964. https://doi.org/10.1016/j.apsusc.2023.156964

Garcia-Banos B, Reinosa JJ, Penaranda-Foix FL, Fernandez JF, Catala-Civera JM (2019) Temperature assessment of microwave-enhanced heating processes. Sci Rep 9(1):10809. https://doi.org/10.1038/s41598-019-47296-0

Guo RT, Wang J, Bi ZX, Chen X, Hu X, Pan WG (2023) Recent advances and perspectives of core–shell nanostructured materials for photocatalytic CO(2) reduction. Small 19(9):e2206314. https://doi.org/10.1002/smll.202206314

Horikoshi S, Serpone N (2014) Role of microwaves in heterogeneous catalytic systems. Catal Sci Technol 4(5):1197. https://doi.org/10.1039/C3CY00753G

Horikoshi S, Osawa A, Sakamoto S, Serpone N (2013) Control of microwave-generated hot spots. Part V. Mechanisms of hot-spot generation and aggregation of catalyst in a microwave-assisted reaction in toluene catalyzed by Pd-loaded AC particulates. Appl Catal A Gen 460(2013):52–60. https://doi.org/10.1016/j.apcata.2013.04.022

Horikoshi S, Kamata M, Mitani T, Serpone N (2014) Control of Microwave-generated hot spots. 6. Generation of hot spots in dispersed catalyst particulates and factors that affect catalyzed organic syntheses in heterogeneous media. Ind Eng Chem Res 53(39):14941–14947. https://doi.org/10.1021/ie502169z

Hu J, Wildfire C, Stiegman AE, Dagle RA, Shekhawat D, Abdelsayed V, Bai X, Tian H, Bogle MB, Hsu C, Luo Y, Davidson SD, Wang Y (2020) Microwave-driven heterogeneous catalysis for activation of dinitrogen to ammonia under atmospheric pressure. Chem Eng J 397:125388. https://doi.org/10.1016/j.cej.2020.125388

Huang J, Zhang H, Tan Q, Li L, Xu R, Xu Z, Li X (2021) Enhanced conversion of CO_2 into O_2-free fuel gas via the Boudouard reaction with biochar in an atmospheric plasmatron. J CO2 Util 45:101429. https://doi.org/10.1016/j.jcou.2020.101429

Hunt J, Ferrari A, Lita A, Crosswhite M, Ashley B, Stiegman AE (2013) Microwave-specific enhancement of the carbon-carbon dioxide (Boudouard) reaction. J Phys Chem C 117(51):26871–26880. https://doi.org/10.1021/JP4076965

Ishida H, Machan C, Robert M, Iwasawa N (2020) Editorial: molecular catalysts for CO_2 fixation/reduction. Front Chem 8:59. https://doi.org/10.3389/fchem.2020.00059

Jia Z, Lin K, Wu G, Xing H, Wu H (2018) Recent progresses of high-temperature microwave-absorbing materials. Nano 13(06):1830005. https://doi.org/10.1142/S1793292018300050

Jin S, Hao Z, Zhang K, Yan Z, Chen J (2021) Advances and challenges for the electrochemical reduction of CO_2 to CO: from fundamentals to industrialization. Angew Chem Int Ed Engl 60(38):20627–20648. https://doi.org/10.1002/anie.202101818

Kappe CO (2004) Controlled microwave heating in modern organic synthesis. Angew Chem Int Ed Engl 43(46):6250–6284. https://doi.org/10.1002/anie.200400655

Ku HS, Siores E, Ball JAR (2012) Application of variable frequency microwave (VFM) to adhesives. J Electromagn Waves Appl 19(11):1467–1484. https://doi.org/10.1163/156939305775701903

Lahijani P, Mohammadi M, Zainal ZA, Mohamed AR (2015a) Advances in CO_2 gasification reactivity of biomass char through utilization of radio frequency irradiation. Energy 93:976–983. https://doi.org/10.1016/j.energy.2015.09.092

Lahijani P, Mohammadi M, Zainal ZA, Mohamed AR (2015b) Improvement of biomass char-CO_2 gasification reactivity using microwave irradiation and natural catalyst. Thermochim Acta 604:61–66. https://doi.org/10.1016/j.tca.2015.01.016

Lahijani P, Zainal ZA, Mohammadi M, Mohamed AR (2015c) Conversion of the greenhouse gas CO_2 to the fuel gas CO via the Boudouard reaction: a review. Renew Sustain Energy Rev 41:615–632. https://doi.org/10.1016/j.rser.2014.08.034

Lam SS, Russell AD, Lee CL, Chase HA (2012) Microwave-heated pyrolysis of waste automotive engine oil: Influence of operation parameters on the yield, composition, and fuel properties of pyrolysis oil. Fuel 92(1):327–339. https://doi.org/10.1016/j.fuel.2011.07.027

Liu H, Wang L (2021) Highly dispersed and stable Ni/SBA-15 catalyst for reverse water-gas shift reaction. Crystals 11(7):790. https://doi.org/10.3390/cryst11070790

Luo J, Gong G, Ma R, Sun S, Cui C, Cui H, Sun J, Ma N (2023) Study on high-value products of waste plastics from microwave catalytic pyrolysis: construction and performance evaluation of advanced microwave absorption-catalytic bifunctional catalysts. Fuel 346:128296. https://doi.org/10.1016/j.fuel.2023.128296

Ma F, Ma D, Wu G, Geng W, Shao J, Song S, Wan J, Qiu J (2016a) Construction of 3D nanostructure hierarchical porous graphitic carbons by charge-induced self-assembly and nanocrystal-assisted catalytic graphitization for supercapacitors. Chem Commun (Camb) 52(40):6673–6676. https://doi.org/10.1039/C6CC02147F

Ma Y-Z, Yu B-J, Guo Y, Wang C-Y (2016b) Facile synthesis of biomass-derived hierarchical porous carbon microbeads for supercapacitors. J Solid State Electrochem 20(8):2231–2240. https://doi.org/10.1016/j.jallcom.2021.161014

MarcoKeiluweit PSN, Johnson MG, Kleber M (2010) Dynamic molecular structure of MPlant biomass-derived black carbon. Biochar Environ Sci Technol. 44:7. https://doi.org/10.1021/es9031419

Medrano-García JD, Ruiz-Femenia R, Caballero JA (2019) Optimal carbon dioxide and hydrogen utilization in carbon monoxide production. J CO2 Util 34:215–230. https://doi.org/10.1016/j.jcou.2019.05.005

Menéndez JA, Dominguez A, Fernández Y, Pis JJ (2007) Evidence of self-gasification during the microwave-induced pyrolysis of coffee hulls. Energy Fuels 21:373–378. https://doi.org/10.1021/ef060331i

Menéndez JA, Juárez-Pérez EJ, Ruisánchez E, Bermúdez JM, Arenillas A (2011) Ball lightning plasma and plasma arc formation during the microwave heating of carbons. Carbon 49(1):346–349. https://doi.org/10.1016/j.carbon.2010.09.010

Snoeckx R, Setareh M, Aerts R, Simon P, Maghari A, Bogaerts A (2013) Influence of N_2 concentration in a CH_4/N_2 dielectric barrier discharge used for CH_4 conversion into H_2. Int J Hydrogen Energy 38(36):16098–16120. https://doi.org/10.1016/j.ijhydene.2013.09.136

Sun J, Wang W, Yue Q, Ma C, Zhang J, Zhao X, Song Z (2016) Review on microwave–metal discharges and their applications in energy and industrial processes. Appl Energy 175:141–157. https://doi.org/10.1016/j.apenergy.2016.04.091

Suttisawat Y, Horikoshi S, Sakai H, Rangsunvigit P, Abe M (2012) Enhanced conversion of tetralin dehydrogenation under microwave heating: effects of temperature variation. Fuel Process Technol 95:27–32. https://doi.org/10.1016/j.fuproc.2011.11.006

Thostenson ET, Chou T-W (1999) Microwave processing: fundamentals and applications. Composites Part A Appl Sci 30:17. https://doi.org/10.1016/S1359-835X(99)00020-2

Tiwari S, Caiola A, Bai X, Lalsare A, Hu J (2019) Microwave plasma-enhanced and microwave heated chemical reactions. Plasma Chem Plasma Process 40(1):1–23. https://doi.org/10.1007/s11090-019-10040-7

Tsukahara Y, Higashi A, Yamauchi T, Nakamura T, Yasuda M, Baba A, Wada Y (2010) In situ observation of nonequilibrium local heating as an origin of special effect of microwave on chemistry. J Phys Chem C 114:5. https://doi.org/10.1021/jp100509h

Vakalis S, Heimann R, Ahmad J, Patuzzi F, Baratieri M (2018) The case of Frictional Torrefaction and the effect of reflux condensation on the operation of the Rotary Compression Unit. Bioresour Technol 268:91–96. https://doi.org/10.1016/j.biortech.2018.07.140

Wang D-W, Li F, Liu M, Lu GQ, Cheng H-M (2008) 3D aperiodic hierarchical porous graphitic carbon material for high-rate electrochemical capacitive energy storage. Angew Chem 120(2):379–382. https://doi.org/10.1002/anie.200702721

Wang W, Wang L, Su W, Xing Y (2022) Photocatalytic CO_2 reduction over copper-based materials: a review. J CO2 Util 61:102056. https://doi.org/10.1016/j.jcou.2022.102056

Wu Z, Tian K, Huang T, Hu W, Xie F, Wang J, Su M, Li L (2018) Hierarchically porous carbons derived from biomasses with excellent microwave absorption performance. ACS Appl Mater Interfaces 10(13):11108–11115. https://doi.org/10.1021/acsami.7b17264

Xuan X, Jiang K, Huang S, Feng B, Qiu F, Han S, Zhu J, Zhuang X (2022) Tertiary amine-functionalized Co(II) porphyrin to enhance the electrochemical CO_2 reduction activity. J Mater Sci 57(22):10129–10140. https://doi.org/10.1007/s10853-022-07303-8

Yuan X, Lee JG, Yun H, Deng S, Kim YJ, Lee JE, Kwak SK, Lee KB (2020) Solving two environmental issues simultaneously: waste polyethylene terephthalate plastic bottle-derived microporous carbons for capturing CO_2. Chem Eng J 397:125350. https://doi.org/10.1016/j.cej.2020.125350

Yuan X, Suvarna M, Low S, Dissanayake PD, Lee KB, Li J, Wang X, Ok YS (2021) Applied machine learning for prediction of CO_2 adsorption on biomass waste-derived porous carbons. Environ Sci Technol 55(17):11925–11936. https://doi.org/10.1021/acs.est.1c01849

Yuan X, Cao Y, Li J, Patel AK, Dong CD, Jin X, Gu C, Yip ACK, Tsang DCW, Ok YS (2023) Recent advancements and challenges in emerging applications of biochar-based catalysts. Biotechnol Adv 67:108181. https://doi.org/10.1016/j.biotechadv.2023.108181

Zhai R, Zhang L, Gu M, Zhao X, Zhang B, Cheng Y, Zhang J (2023) A review of phosphorus structures as CO(2) reduction photocatalysts. Small 19(19):e2207840. https://doi.org/10.1002/smll.202207840

Zhang Y, Geng P, Zheng Y (2019) Exploration and practice to improve the kinetic analysis of char-CO_2 gasification via thermogravimetric analysis. Chem Eng J 359:298–304. https://doi.org/10.1016/j.cej.2018.11.122

Zhao K, Quan X (2021) Carbon-based materials for electrochemical reduction of CO_2 to C2+ oxygenates: recent progress and remaining challenges. ACS Catal 11(4):2076–2097. https://doi.org/10.1021/acscatal.0c04714